HAL QCD potentials with non-zero total momentum and an application to the $I = 2\,\pi\pi$ scattering

Sinya Aoki[a,b,*] **and Yutaro Akahoshi**[a,b]

[a]*Center for Gravitational Physics, Yukawa Institute for Theoretical Physics, Kyoto University, Kitashirakawa Oiwakecho, Sakyo-ku, Kyoto 606-8502, Japan*

[b]*Riken Nishina Center (RNC), Hirosawa 2-1, Wako, Saitama 351-0198, Japan*

E-mail: saoki@yukawa.kyoto-u.ac.jp, yutaro.akahoshi@yukawa.kyoto-u.ac.jp

We consider the HAL QCD method in the system with non-zero total momentum (laboratory frame). We derive a relation between the NBS wave function in the laboratory frame and the energy-independent non-local potential (HAL QCD potential), and propose the time-dependent method to extract the potential from correlation functions in the laboratory frame. We then apply this formulation to the $I = 2\,\pi\pi$ system to calculate the corresponding potential in the laboratory frame, employing the 2+1 flavor gauge configuration on a $32^3 \times 64$ lattice at the lattice spacing $a \simeq 0.091$ fm and $m_\pi \simeq 700$ MeV. While statistical errors are larger, the effective leading order (LO) potentials and corresponding phase shift agree with those from the HAL QCD potential in the center of mass (CM) frame. We also demonstrate the consistency in scattering phase shifts between the HAL QCD method in several frames and the finite volume method. The HAL QCD method in the laboratory frame enlarges applicabilities of the method to investigate hadron interaction including mesonic resonances such as ρ and σ.

---

*Speaker

1. Introduction

Hadron interactions have been investigated actively in lattice QCD mainly by two methods, the finite volume method[1–3] and the HAL QCD method[4–7], both of which are based on the fact that the Nambu-Bethe-Salpeter (NBS) wave functions contains information of the scattering S-matrix in QCD.

The HAL QCD method works well, in particular for two baryon interactions (see [8] and references therein), thanks to the time-dependent method[7] and multi-channel extension[9]. Recently, resonances such as the ρ meson have been investigated in the HAL QCD method, by various improvements for all-to-all propagators[10–14]. If we extend the HAL QCD method to systems having the same quantum numbers of the QCD vacuum such as the σ meson, a serious obstruction appears. For example, the vacuum contribution dominates over signals for $\pi\pi$ states in the correlation function between σ resonance and the $I = 0$ S-wave $\pi\pi$ in the center of mass frame as

$$\langle 0|\pi(t)\pi(t)\sigma(0)|0\rangle \simeq \langle 0|\pi(t)\pi(t)|0\rangle\langle 0|\sigma(0)|0\rangle + e^{-2m_\pi t}\langle 0|\pi(t)\pi(t)|\pi\pi\rangle\langle\pi\pi|\sigma(0)|0\rangle + \cdots . \quad (1)$$

An introduction of non-zero total momenta to the system is a promising way to remove this type of contaminations from the vacuum, and the theoretical formulation for the HAL QCD method in the laboratory system has already been proposed[15]. Recently, we have performed a numerical test of the formulation to extract the potential from the $I = 2$ $\pi\pi$ system in the laboratory frame, which is reported here. After briefly explaining the general formulation, we present numerical results. The $I = 2$ $\pi\pi$ scattering phase shift obtained in the laboratory frame are compared with those from the potential in the CM frame as well as the finite volume spectra.

2. Formulation for the HAL QCD potential in the laboratory frame

2.1 Lorentz transformation for the NBS wave function

The NBS wave function for a scalar theory in the Minkowski spacetime is defined in a general frame as

$$\psi_{k_1,k_2}(x_1, x_2) = \langle 0|T\{\phi(x_1)\phi(x_2)\}|k_1, k_2\rangle := \varphi_{k_1,k_2}(x)e^{-iWX^0+i\mathbf{P}\cdot\mathbf{X}}, \quad (2)$$

where $\phi(x)$ is a scalar field operator, $|k_1, k_2\rangle$ is an asymptotic in-state of two particles with four momenta k_1 and k_2, $W := \sqrt{\mathbf{k}_1^2 + m^2} + \sqrt{\mathbf{k}_2^2 + m^2}$ and $\mathbf{P} := \mathbf{k_1} + \mathbf{k_2}$ are the total energy and momentum, respectively, while $X := (x_1 + x_2)/2$ and $x := x_1 - x_2$ are center of gravity and relative coordinates, respectively, and $\varphi_{k_1,k_2}(x)$ is a relative NBS wave function.

The relative NBS wave function in the laboratory frame is related to the one in the CM frame as $\varphi_{k_1,k_2}(x) = \varphi_{k_1^*,k_2^*}(x^*)$, where quantities with $*$ represent those in the CM frame, and are related to those without it in the laboratory frame as $x^{*0} = \gamma(x^0 - \mathbf{v}\cdot\mathbf{x}_\parallel)$, $\mathbf{x}_\parallel^* = \gamma(\mathbf{x}_\parallel - \mathbf{v}x^0)$, $\mathbf{x}_\perp^* = \mathbf{x}_\perp$. Here $\parallel$ and $\perp$ means vectors parallel and perpendicular to $\mathbf{v} := \mathbf{P}/W$, respectively. The boost factor γ is given by $\gamma := \frac{1}{\sqrt{1-\mathbf{v}^2}}$, $W^{*2} = W^2 - \mathbf{P}^2$, and $\mathbf{P}^* = 0$ by definition.

2.2 Potential from the NBS wave function in the laboratory frame

The HAL QCD potential is defined in the CM frame, and is extracted from the correlation functions in the Euclidean spacetime by the Wick rotation as $x^4 = ix^0$, which leads to $x^{*4} = \gamma(x^4 - i\mathbf{v}\cdot\mathbf{x}_\parallel)$, $\mathbf{x}_\parallel^* = \gamma(\mathbf{x}_\parallel + i\mathbf{v}x^4)$, $\mathbf{x}_\perp^* = \mathbf{x}_\perp$.

The NBS wave function is related to the non-local potential in the derivative expansion as

$$\frac{1}{2\mu}(\nabla^{*2} + \mathbf{k}^{*2})\varphi_{k_1^*,k_2^*}(\mathbf{x}^*, x^{*4}) = \sum_{j=0}^{\infty} V_{x^{*4}}^j(\mathbf{x}^*)\left(\nabla^{*2}\right)^j \varphi_{k_1^*,k_2^*}(\mathbf{x}^*, x^{*4}), \tag{3}$$

where $\mu = m/2$ is the reduced mass and the subscript x^{*4} of V^j represents the scheme to define the potential with the relative Euclidean time separation x^{*4}. (Usually, the potential is defined at the equal time, $x^{*4} = 0$.)

Using $\varphi_{k_1^*,k_2^*}(\mathbf{x}^*, x^{*4}) = \varphi_{k_1,k_2}(\mathbf{x}, x^4)$ and (3), we obtain[15]

$$\frac{1}{2\mu}\left(\nabla^{*2} + \mathbf{k}^{*2}\right)\varphi_{k_1,k_2}(\mathbf{x}, x^4) = \sum_{j=0}^{\infty} V_{\gamma(x^4 - i\mathbf{v}\cdot\mathbf{x}_\parallel)}^j\left(\mathbf{x}_\perp, \gamma(\mathbf{x}_\parallel + i\mathbf{v}x^4)\right)\left(\nabla^{*2}\right)^n \varphi_{k_1,k_2}(\mathbf{x}, x^4), \tag{4}$$

where $\nabla^{*2} = \nabla_\perp^2 + \gamma^2(\nabla_\parallel + i\mathbf{v}\partial_{x^4})^2$ and $\mathbf{k}^{*2} = W/4 - m^2$.

Since $\mathbf{x}^*_\parallel$ becomes complex for non-zero x^4, a meaningful potential is obtained from (4) only at $x^4 = 0$. In addition, we take $\mathbf{x}_\parallel = 0$ to extract the equal time scheme potential. For example, the effective LO potential in the equal time scheme becomes[15]

$$V_{x^{*4}=0}^{\mathrm{LO}}(\mathbf{x}^*_\perp = \mathbf{x}_\perp, \mathbf{x}^*_\parallel = 0) = \left.\frac{\left\{\nabla_\perp^2 + \gamma^2(\nabla_\parallel + i\mathbf{v}\partial_{x^4})^2 + \mathbf{k}^{*2}\right\}\varphi_{k_1,k_2}(\mathbf{x}, x^4)}{2\mu\varphi_{k_1,k_2}(\mathbf{x}, x^4)}\right|_{x^4=0, \mathbf{x}_\parallel=0}, \tag{5}$$

where we set $x^4 = 0$ and $\mathbf{x}_\parallel = 0$ after taking derivatives in the right-hand side.

2.3 Time-dependent method in the laboratory frame

For the extraction of the potential, we employ the time-dependent HAL QCD method[7], which is given in the CM frame as

$$V_{x^{*4}}^{\mathrm{LO}}(\mathbf{x}^*)R(\mathbf{x}^*, x^{*4}, X^{*4}) = \left(\frac{\nabla^{*2}}{2\mu} - \partial_{X^{*4}} + \frac{1}{4m}\partial_{X^{*4}}^2\right)R(\mathbf{x}^*, x^{*4}, X^{*4}), \tag{6}$$

where R is the 4-pt function divided by the 2-pt function squared, expressed by

$$R(\mathbf{x}^*, x^{*4}, X^{*4}) = \sum_n A_n\varphi_{W_n^*}(\mathbf{x}^*, x^{*4})e^{-(W_n^* - 2m)X^{*4}} + \cdots, \quad W_n^* := 2\sqrt{\mathbf{k}_n^{*2} + m^2}, \tag{7}$$

A_n is an overlapping of the n-th eigenstate to the source operator, and ellipses represent inelastic contributions.

The time-dependent formula in the laboratory frame is more involved, and is given by[15]

$$V_{x^{*4}=0}^{\mathrm{LO}}(\mathbf{x}^*_\perp = \mathbf{x}_\perp, \mathbf{x}^*_\parallel = 0) = \left.\frac{(L_\perp + L_\parallel + mE)(\mathbf{x}, x^4, X^4)}{mG(\mathbf{x}, x^4, X^4)}\right|_{x^4=0, \mathbf{x}_\parallel=0}, \tag{8}$$

where

$$G(\mathbf{x}, x^4, X^4) = \left[(\partial_{X^4} - 2m)^2 - \mathbf{P}^2\right]R(\mathbf{x}, x^4, X^4), \tag{9}$$

$$E(\mathbf{x}, x^4, X^4) = \left[\frac{\partial_{X^4}^2}{4m} - \partial_{X^4} - \frac{\mathbf{P}^2}{4m}\right]G(\mathbf{x}, x^4, X^4), \quad L_\perp(\mathbf{x}, x^4, X^4) = \nabla_\perp^2 G(\mathbf{x}, x^4, X^4), \tag{10}$$

$$L_\parallel(\mathbf{x}, x^4, X^4) = \left[-(\partial_{X^4} - 2m)\nabla_\parallel + i\mathbf{P}\partial_{x^4}\right]^2 R(\mathbf{x}, x^4, X^4). \tag{11}$$

Note that the right-hand side in (8) are written in terms of quantities in the laboratory frame only, while the potential in the left-hand side is defined in the CM frame.

3. Numerical results for the $I = 2$ $\pi\pi$ system

We apply the formula in the laboratory frame to the $I = 2$ $\pi\pi$ system for the demonstration.

3.1 Simulation details

We employ the 2+1 flavor ensemble generated by the CP-PACS collaboration[16] on a $32^3 \times 64$ lattice with the Iwasaki gauge action at $\beta = 1.90$, the non-perturbatively $O(a)$ improved Wilson action at $c_{\text{SW}} = 1.7150$ and hopping parameters $(\kappa_{ud}, \kappa_s) = (0.13700, 0.13640)$, which leads to $a \simeq 0.091$ fm for the lattice spacing and $m_\pi \simeq 700$ MeV for the pion mass. All correlation functions are evaluated by the one-end trick[17] on 399 configurations $\times$ 16 source time locations with the periodic boundary condition in all directions, and their errors are estimated by the jack-knife method with bin size 21. A single Z_4 noise is used in the one-end trick with dilutions for color, spinor and even/odd spatial indices. Quark sources are smeared as $q_s(\mathbf{x}, t) = \sum_{\mathbf{y}} f(\mathbf{x} - \mathbf{y}) q(\mathbf{y}, t)$ with the Coulomb gauge fixing, where the smearing function is given by $f(\mathbf{x}) = Ae^{-B|\mathbf{x}|}$ with $B = 0.3$. We take $A = 1$ for $|\mathbf{x}| = 0$, $A = 1.2$ for $|\mathbf{x}| < \frac{L-1}{2}$ with $L = 32$, or $A = 0$ otherwise. We consider two laboratory frames, the case 1 with $\mathbf{P} = (0, 0, 2\pi/L)$, where pions have momenta $\mathbf{P}$ and $\mathbf{0}$, and the case 2 with $\mathbf{P} = (0, 0, 4\pi/L)$, where each pion has a momentum $\mathbf{P}/2$. In addition, we also consider the CM frame ($\mathbf{P} = (0, 0, 0)$) for comparisons.

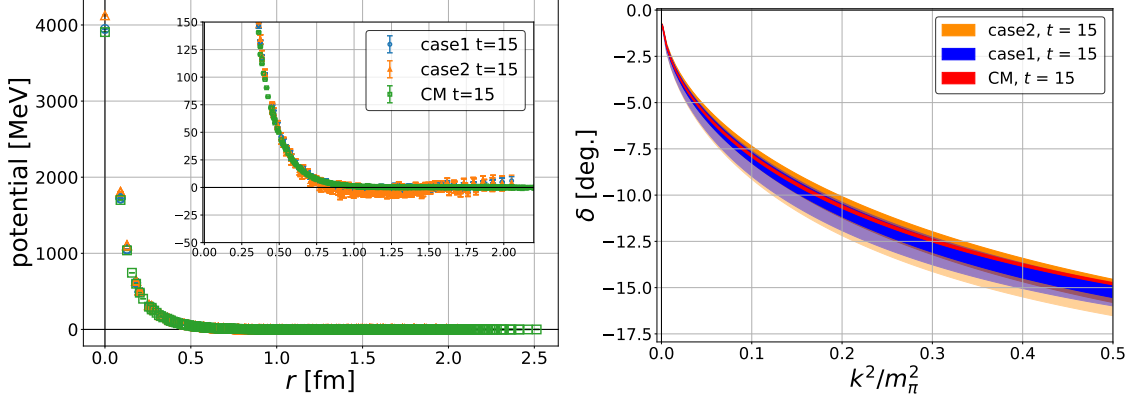### 3.2 $I = 2$ $\pi\pi$ Potentials and scattering phase shifts
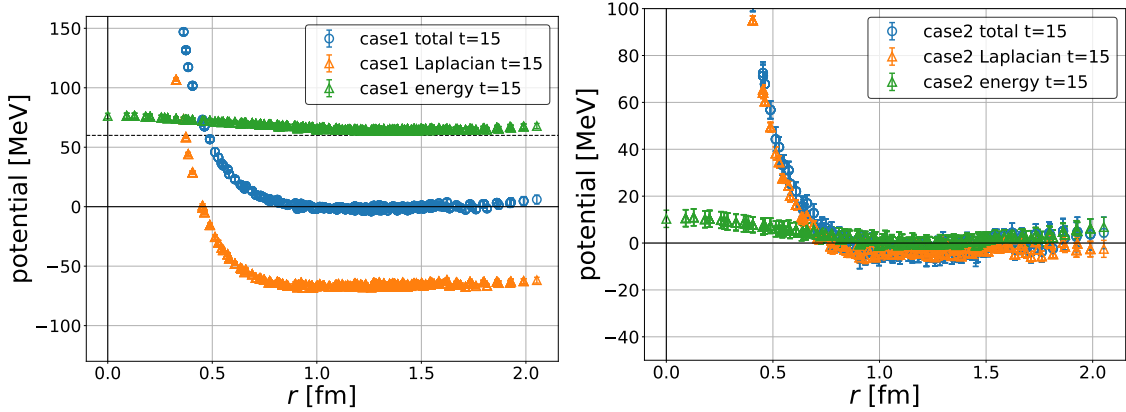
Figure 1: Decompositions of the effective LO potential in case 1 (Left) and case 2 (Right), where dotted lines represent expected relative energies in non-interacting cases.

Fig. 1 shows the effective LO potential and its decomposition at $t = X^4 = 15$ for the case 1 (Left) and the case 2 (Right), which is given by

$$V_{x^{*4}=0}^{\text{LO}}(\mathbf{x}_\perp^* = \mathbf{x}_\perp, \mathbf{x}_\parallel^* = 0) = \left.\frac{(L_\perp + L_\parallel)(\mathbf{x}, x^4, X^4)}{mG(\mathbf{x}, x^4, X^4)}\right|_{x^4=0, \mathbf{x}_\parallel=0} + \left.\frac{E(\mathbf{x}, x^4, X^4)}{G(\mathbf{x}, x^4, X^4)}\right|_{x^4=0, \mathbf{x}_\parallel=0}, \quad (12)$$

where the first term represents the Laplacian contribution (orange triangles), the second one the kinetic energy contribution (green triangles), and their sum is the effective LO potential (blue circles). For the case 1 (Left), the large negative shift from zero of the Laplacian contribution at

long distances is compensated by the large positive shift of the kinetic energy contribution, which is dominated by the ground state in this laboratory frame (dotted line in the figure for the non-interacting case), so that the total potential approaches to zero at long distances. This cancellation between the Laplacian and kinetic energy contributions is an evidence for the validity of the time dependent method complicated in the laboratory frame. For the case 2 (Right), on the other hand, these shifts at long distances are small, as an expected kinetic energy for the ground state is almost zero.

Figure 2: (Left) A comparison of the effective LO potentials among the case 1 (blue circles), the case 2 (orange triangles) and the CM (green squares). An inset shows its enlargement. (Right) Scattering phases shifts $\delta_0(k)$ for the $I = 2$ $\pi\pi$ system as a function of k^2/m_π^2 for the case 1 (blue), case 2 (orange) and the CM (red), where dark and light color bands show statistical and systematic errors, respectively.

In Fig. 2 (Left), we compare the effective LO potentials among the case 1 (blue circles), the case 2 (orange triangles) and the CM (green squares), which are almost identical except at short distances though statistical fluctuations are much larger in laboratory frames. Larger statistical fluctuations may be caused by larger total momentum **P**, as similar phenomena have been observed for single hadron energies with non-zero momenta in lattice QCD. Larger fluctuations may be explained partly by larger contaminations to the $L = 0$ contribution from higher partial waves in the laboratory frame with $L = 2, 4, \cdots$, while contaminations come from $L = 4, 6, \cdots$ in the CM frame. The effective LO potentials show the interaction between $I = 2$ $\pi\pi$ is repulsive at all distances.

We next calculate scattering phase shift $\delta_0(k)$ for the $I = 2$ $\pi\pi$ system, using these three potentials fitted by a sum of 4 Gaussian functions. While central values of scattering phase shifts are obtained form potentials at $X^4 = 15$, their systematic uncertainties are estimated by differences between $X^4 = 15 \pm 1$. Fig. 2 (Right) shows scattering phase shifts $\delta_0(k)$ as a function of k^2/m_π^2 for the case 1 (blue), case 2 (orange) and the CM frame (red), where statistical and systematic errors are given by dark and light color bands, respectively. As expected from results for potentials, we observe that all three cases give consistent results though both statistical and systematic errors increases for larger total momentum **P**. Form this agreement, we conclude that hadron interactions can be investigated by the HAL QCD method using the laboratory frame in practice, even though systematic as well as statistical errors become larger.
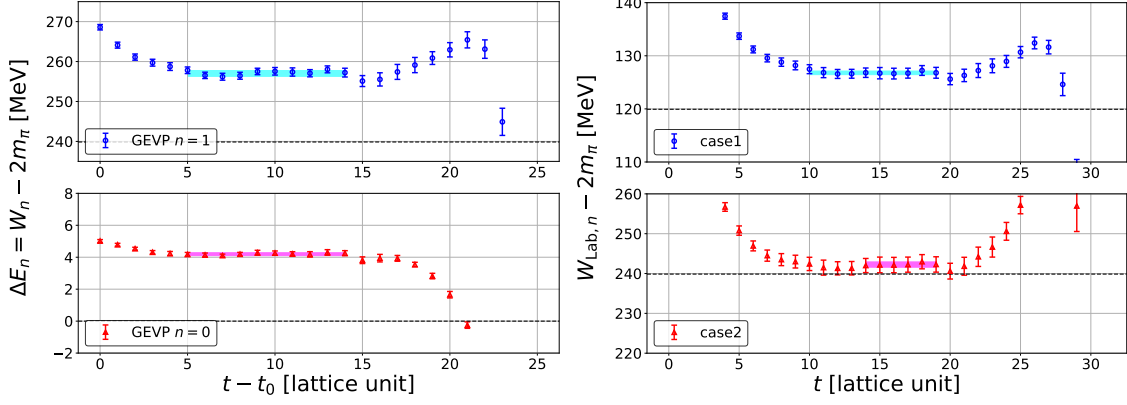
Figure 3: (Left) Effective energies of the $I = 2$ $\pi\pi$ system, obtained by eigenvalues of the correlation matrix in the CM frame for the ground state (red triangles) and the first excited state (blue circles). Fits with a single exponential and the corresponding fit ranges are shown by color bands. (Right) Effective energies and their single exponential fits for the ground state of the $I = 2$ $\pi\pi$ system in the laboratory frames for the case 1 (blue circles) and the case 2 (red triangles). Dashed and dotted lines are the ground state energies for non-interacting cases.

3.3 Comparisons with the finite volume method

We here compare our results to those obtained by the Lüscher's finite volume method. We calculate finite volume spectra from correlations functions, two (the ground and the first excited energies) in the CM frame, one each (the ground state) in the case 1 and the case 2. Fig. 3 (Left) shows effective energies of the $I = 2$ $\pi\pi$ system for the grand state (red triangles) and the first excited states (blue circles) obtained by the variational method in the CM frame, while Fig. 3 (Right) presents effective energies for the grand state in the case 1 (blue circles) and in the case 2 (red triangles).
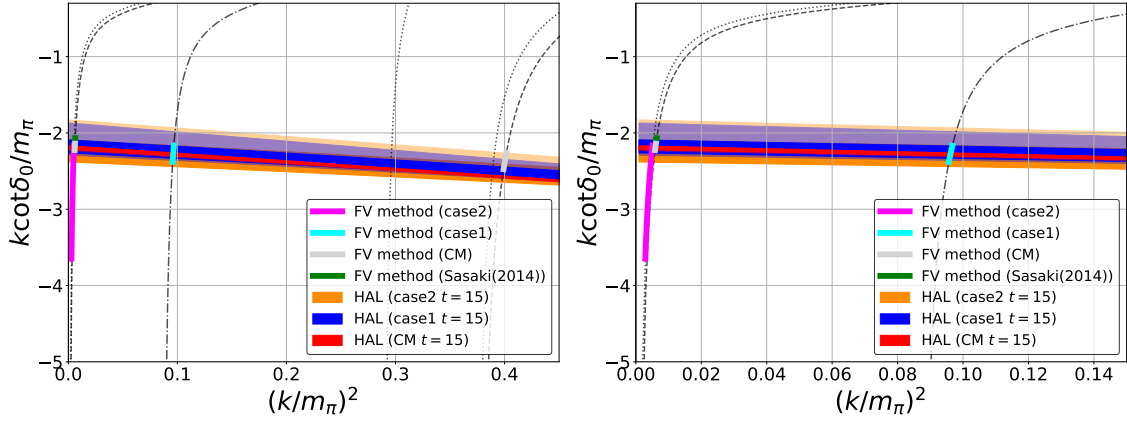
Figure 4: (Left) A comparison of $k \cot \delta_0(k)$ with results from the Lüscher's finite volume method in the casde 1 (cyan), the case 2 (magenta), the CM frame (gray), together with the result from [18] in the CM frame (green). Dash-dot, dotted, and dashed lines represent constraints by the Lüscher's formula in the case 1, the case 2, and the CM, respectively. (Right) The enraged one in the low energy region.

Fig.4 summarizes all results in terms of $k \cot \delta_0(k)/m_\pi$ as a function k^2/m_π^2, where the HAL

QCD results are given by red (CM), blue (case 1) and orange (case) bands representing statistical (dark) and systematic (light) errors, while results from the finite volume spectra are shown by white (CM), cyan (case 1) and magenta (case 2) bands, together with the CM result from [18] by a green band. In the figure, constraints by the Lüscher's finite volume formula are represented by dashed (CM), dash-dot (case 1) and dotted (case 2) lines. Since finite volume data must lie on these lines, errors of k sometimes result in large errors of $k \cot \delta_0(k)$, as seen in the case 2 (magenta band).

Although errors are larger for both HAL QCD and finite volume data in laboratory frames, we confirm that $k \cot \delta_0(k)$ by the HAL QCD potential method are consistent with those by the finite volume method. These agreements support not only that the HAL QCD method in the laboratory frame works in practice for this system, but also that the HAL QCD method and the finite volume method agree with each other.

4. Summary

In this talk, we apply the HAL QCD method with non-zero total momentum to the $I = 2$ $\pi\pi$ system. We show that the method works in practice and gives reasonable results. This is encouraging since the method opens new possibilities to extract potential of the system with the same quantum number to the vacuum state such as the $I = 0$ S-wave $\pi\pi$ system, which contains the σ resonance.

References

[1] M. Luscher, Nucl. Phys. B **354**, 531 (1991).

[2] K. Rummukainen and S. A. Gottlieb, Nucl. Phys. B **450**, 397 (1995) [hep-lat/9503028].

[3] M. T. Hansen and S. R. Sharpe, Phys. Rev. D **86**, 016007 (2012) [arXiv:1204.0826 [hep-lat]].

[4] N. Ishii, S. Aoki and T. Hatsuda, Phys. Rev. Lett. **99**, 022001 (2007) [nucl-th/0611096].

[5] S. Aoki, T. Hatsuda and N. Ishii, Prog. Theor. Phys. **123**, 89 (2010) [arXiv:0909.5585 [hep-lat]].

[6] S. Aoki, Prog. Part. Nucl. Phys. **66**, 687 (2011) [arXiv:1107.1284 [hep-lat]].

[7] N. Ishii *et al.* , Phys. Lett. B **712**, 437 (2012) [arXiv:1203.3642 [hep-lat]].

[8] S. Aoki and T. Doi, Front. in Phys. **8** (2020), 307 doi:10.3389/fphy.2020.00307 [arXiv:2003.10730 [hep-lat]].

[9] S. Aoki *et al.* , Proc. Japan Acad. B **87** (2011), 509-517 doi:10.2183/pjab.87.509 [arXiv:1106.2281 [hep-lat]].

[10] D. Kawai *et al.* , PTEP **2018**, no. 4, 043B04 (2018) [arXiv:1711.01883 [hep-lat]].

[11] D. Kawai, EPJ Web Conf. **175**, 05007 (2018).

[12] Y. Akahoshi, S. Aoki, T. Aoyama, T. Doi, T. Miyamoto and K. Sasaki, PTEP **2019** (2019) no.8, 083B02 doi:10.1093/ptep/ptz078 [arXiv:1904.09549 [hep-lat]].

[13] Y. Akahoshi, S. Aoki, T. Aoyama, T. Doi, T. Miyamoto and K. Sasaki, PTEP **2020** (2020) no.7, 073B07 doi:10.1093/ptep/ptaa087 [arXiv:2004.01356 [hep-lat]].

[14] Y. Akahoshi, S. Aoki and T. Doi, Phys. Rev. D **104** (2021) no.5, 054510 doi:10.1103/PhysRevD.104.054510 [arXiv:2106.08175 [hep-lat]].

[15] S. Aoki, PoS **LATTICE2019** (2019), 020 doi:10.22323/1.363.0020 [arXiv:2001.01076 [hep-lat]].

[16] S. Aoki *et al.*, Phys. Rev. D **79** (2009), 034503 doi:10.1103/PhysRevD.79.034503 [arXiv:0807.1661 [hep-lat]].

[17] C. McNeile *et al.*, Phys. Rev. D **73** (2006), 074506 doi:10.1103/PhysRevD.73.074506 [arXiv:hep-lat/0603007 [hep-lat]].

[18] K. Sasaki *et al.* , Phys. Rev. D **89** (2014) no.5, 054502 doi:10.1103/PhysRevD.89.054502 [arXiv:1311.7226 [hep-lat]].

[19] T. Amagasa et al., *Sharing lattice QCD data over a widely distributed file system*, *J. Phys. Conf. Ser.* **664** (2015) 042058.

[20] S. Ueda, S. Aoki, T. Aoyama, K. Kanaya, H. Matsufuru, S. Motoki et al., *Development of an object oriented lattice QCD code 'Bridge++'*, *J. Phys. Conf. Ser.* **523** (2014) 012046.

[21] I. Kanamori and H. Matsufuru, *Practical Implementation of Lattice QCD Simulation on SIMD Machines with Intel AVX-512*, *Lect. Notes Comput. Sci.* **10962** (2018) 456 [1811.00893].